

Effects of Artificial Collisions, Filtering, and Nonlocal Closure Approaches on Hermite-based Vlasov-Poisson Simulations

Opal Issan^{a,b,*}, Oleksandr Chapurin^b, Oleksandr Koshkarov^b, Gian Luca Delzanno^b

^a*Department of Mechanical and Aerospace Engineering, University of California San Diego, La Jolla, CA, USA*

^b*T-5 Applied Mathematics and Plasma Physics Group, Los Alamos National Laboratory, Los Alamos, NM, USA*

February 18, 2025

Abstract

Kinetic simulations of collisionless plasmas are computationally challenging due to phase space mixing and filamentation, resulting in fine-scale velocity structures. This study compares three methods developed to reduce artifacts related to limited velocity resolution in Hermite-based Vlasov-Poisson simulations: artificial collisions, filtering, and nonlocal closure approaches. We evaluate each method's performance in approximating the linear kinetic response function and suppressing recurrence in linear and nonlinear regimes. Numerical simulations of Landau damping demonstrate that artificial collisions, particularly higher orders of the Lenard-Bernstein collisional operator, most effectively recover the correct damping rate across a range of wavenumbers. Moreover, Hou-Li filtering and nonlocal closures underdamp high wavenumber modes in linear simulations, and the Lenard-Bernstein collisional operator overdamps low wavenumber modes in both linear and nonlinear simulations. This study demonstrates that hypercollisions offer a robust approach to kinetic simulations, accurately capturing collisionless dynamics with limited velocity resolution.

Keywords: Vlasov-Poisson equations, spectral methods, artificial collisions, filtering, Landau closure

1. Introduction

Kinetic simulations of collisionless plasmas are important for many applications, e.g. astrophysics, geophysics, and laboratory fusion devices. Solving the collisionless Vlasov equation numerically is challenging due to its high dimensionality, Hamiltonian structure, and significant spatial and temporal scale separation. Furthermore, kinetic solvers struggle to accurately capture phase-space mixing, in which the distribution function develops increasingly fine structures in velocity space, known as *filamentation* [1]. As shown by the solution $f(x,v,t) = f(x - vt, v, 0)$ to the free-streaming equation $\partial_t f + v\partial_x f = 0$, these structures cannot be resolved after a finite time determined by the resolution of the velocity space. Filamentation can also cause *recurrence* in Eulerian solvers (grid or spectral), where the solution is artificially periodic in time [2, 3].

A large class of kinetic spectral solvers use Hermite functions in velocity space, weighted by a Gaussian distribution [1, 4–23]. Hermite-based spectral expansions are advantageous for accurately approximating near-Maxwellian distributions with only a few basis functions. However, the spectral method exhibits recurrence phenomena when filamentation develops beyond the scales that the finite Hermite resolution can resolve. An insightful mechanical analogy from Hammett et al. [24] describes the Hermite moment system as a semi-infinite chain of springs and masses. In this analogy, an initial perturbation of the lowest Hermite mode corresponds to displacing the first mass in the chain. Truncating the Hermite system is akin to placing a wall at the end of a finite spring-mass chain. The wall then reflects the perturbation energy, resulting in an inverse cascade from the last mass back to the first that artificially reconstructs the initial perturbation. The recurrence period in Hermite simulations scales with $\sim \sqrt{N_v}/k$ [3], where N_v is the number of Hermite moments and k is the spatial wavenumber of the initial perturbation. In nature, filamentation exhibits a cutoff scale at which diffusive scattering effects become significant. To adequately resolve such scales, a very high resolution in velocity is necessary; for instance, the slow solar wind requires $N_v \sim 1,800$ [19] and tokamak edge simulations require $N_v \sim 180$ [22], which becomes computationally prohibitive for long-time or three-dimensional simulations. Nevertheless, a low-resolution Hermite spectral representation is analogous to assuming that the particle distribution function lacks

*Corresponding author

Email address: oissan@ucsd.edu (Opal Issan)

fine-scale structures in velocity space, which can lead to numerical instabilities in the case of filamentation. This phenomenon is common in other spectral methods, known as *spectral blocking* [25], where noise accumulates in high-order spectral modes near the truncation limit.

The most common closure for the Hermite spectral approximation is closure by truncation, which assumes that the last spectral moment is zero. However, the Landau root [26] does not emerge as a discrete eigenvalue with the closure by truncation, regardless of velocity resolution. Grant and Feix [1] were the first to show that adding artificial collisions to the finite system with the closure by truncation can restore the correct Landau damping [20, 27, 28]. Previous work by [1, 9] use the Lenard Bernstein (LB) [29] collisional operator. Similarly, recent work by [11–13, 15–17, 23] use a hypercollisional operator, which damps more strongly the higher-order Hermite moments in comparison to the LB operator. Filtering techniques, such as Klimas [30] and Hou-Li [31], are also used to suppress recurrence and filamentation artifacts [3, 32–35]. Another method for incorporating kinetic physics into moment solvers is with a linear nonlocal closure, often referred to as *Landau-fluid closures* [36, 37]. This approach matches the closure coefficients to the asymptotic limits of the linear kinetic response function. Landau-fluid closures were initially formulated for fluid models incorporating three and four moments and were later generalized to models involving higher moments in Hermite space [38]. Therefore, it becomes essential to incorporate a modified term or closure that introduces dissipation into the discrete system to prevent filamentation issues while ensuring that the chosen approach accurately captures the system’s average dynamics.

In this paper, we provide a comprehensive comparison of artificial collisions, filtering, and nonlocal closure approaches. We examine the discrete system approximation of the linear kinetic response function and evaluate each method’s ability to recover the Landau damping dispersion relation. Additionally, we assess each method’s suppression of recurrence and filamentation artifacts by simulating a Langmuir wave’s linear and nonlinear Landau damping. This paper builds on previous work by Pezzi et al. [20], which shows that the LB collisional operator significantly modifies the collisionless dynamics. Specifically, at the same collisional rate that recovers the Landau root, nonlinear waves damp due to LB collisions instead of reaching saturation. We replicate these findings and assess whether similar issues arise with hypercollisions, filtering, and nonlocal closure approaches. The analysis shows that hypercollisions, particularly higher orders of the LB collision operator, most effectively recover the correct damping rate across a range of wavenumbers, particularly in limited velocity resolution.

This paper is organized as follows. Section 2 briefly reviews the one-dimensional collisionless Vlasov-Poisson equations, linear theory, and the velocity discretization of the particle distribution function using the asymmetrically weighted Hermite spectral expansion. Section 3 describes the three methods to mitigate recurrence: (1) artificial collisions, (2) filtering, and (3) nonlocal closures, along with their ability to approximate linear kinetic dynamics. We numerically test these methods on the linear and nonlinear Landau damping benchmark problem in section 4, and the concluding remarks are given in section 5.

2. Vlasov-Poisson Equations: Hermite Spectral Discretization in Velocity

We present the one-dimensional collisionless Vlasov-Poisson equations in section 2.1. Section 2.2 derives the well-known linear kinetic response function. We introduce the asymmetrically weighted Hermite expansion and its approximation of the response function in section 2.3.

2.1. Vlasov-Poisson Equations

We consider the one-dimensional Vlasov-Poisson equations, which model the interaction of collisionless charged particles with a self-consistent electric field. The plasma is composed of electrons and immobile background ions. The one-dimensional (normalized) Vlasov-Poisson equations are

$$\left(\frac{\partial}{\partial t} + v \frac{\partial}{\partial x} + \frac{\partial \phi(x, t)}{\partial x} \frac{\partial}{\partial v} \right) f(x, v, t) = 0, \quad (1)$$

$$-\frac{\partial^2 \phi(x, t)}{\partial x^2} = 1 - \int_{\mathbb{R}} f(x, v, t) dv, \quad (2)$$

where $f(x, v, t)$ is the electron distribution function, $\phi(x, t)$ is the electrostatic potential given by $E(x, t) = -\partial \phi(x, t) / \partial x$ such that $E(x, t)$ is the electric field. We consider an unbounded velocity coordinate $v \in \mathbb{R}$, a

periodic spatial coordinate $x \in [0, \ell]$, where ℓ is the length of the spatial domain, and time $t \geq 0$. All quantities in the Vlasov-Poisson equations (1)–(2) are normalized as follows:

$$t := t_d \omega_{pe}, \quad x := \frac{x_d}{\lambda_D}, \quad v := \frac{v_d}{v_{te}}, \quad f := f_d \frac{v_{te}}{n_e}, \quad \phi := \phi_d \frac{e \lambda_D^2}{T_e},$$

where the subscript ‘ d ’ indicates the dimensional quantities, e is the positive elementary charge, $\omega_{pe} := \sqrt{4\pi e^2 n_e / m_e}$ is the electron plasma frequency, m_e is the electron mass, n_e is the reference electron density, $v_{te} := \sqrt{T_e / m_e}$ is the electron thermal velocity, T_e is a reference electron temperature, $\lambda_D := v_{te} / \omega_{pe} = \sqrt{T_e / 4\pi e^2 n_e}$ is the electron Debye length.

2.2. Linear Response Function

The electron distribution function and electrostatic potential can be expressed as the sum of equilibrium and small-amplitude perturbation components

$$\begin{aligned} f(x, v, t) &= f_0(v) + \tilde{f}(x, v, t), & \text{s.t.} & \quad \tilde{f} \ll f_0, \\ \phi(x, t) &= \phi_0(x) + \tilde{\phi}(x, t), & \text{s.t.} & \quad \phi_0(x) = 0. \end{aligned}$$

We are interested in the asymptotic solutions at large times, in which it is sufficient to assume that the first-order perturbed quantities vary as

$$\tilde{f}(x, v, t) = \exp(-i\omega t + ikx) \hat{f}(v) \quad \text{and} \quad \tilde{\phi}(x, t) = \exp(-i\omega t + ikx) \hat{\phi}, \quad (3)$$

where the wavenumber k is real and the frequency $\omega = \omega_r + i\gamma$ is complex; see [39–41] for more details; then $\gamma \in \mathbb{R}$ is the damping/growth rate and $\omega_r \in \mathbb{R}$ is the oscillation frequency. We substitute Eq. (3) into the linearized Vlasov equation (1), resulting in

$$-i\omega \hat{f}(v) + ikv \hat{f}(v) + ik \hat{\phi} \frac{df_0}{dv} = 0 \quad \Rightarrow \quad \hat{f}(v) = k \hat{\phi} \frac{df_0/dv}{\omega - kv}. \quad (4)$$

For a Maxwellian equilibrium, that is, $f_0(v) = \exp(-v^2/2) / \sqrt{2\pi}$, the perturbed density is described via the following linear kinetic response function $R(\xi)$:

$$\hat{n} := \int_{\mathbb{R}} \hat{f}(v) dv = k \hat{\phi} \int_{\mathbb{R}} \frac{df_0/dv}{\omega - kv} dv = \hat{\phi} R(\xi), \quad \text{s.t.} \quad R(\xi) := 1 + \xi Z(\xi) \quad \text{and} \quad \xi := \frac{\omega}{\sqrt{2}|k|}, \quad (5)$$

where the plasma dispersion function is $Z(\xi) = \pi^{-1/2} \int_{\mathbb{R}} \exp(-s^2) / (s - \xi) ds$ for $\text{Im}(\xi) > 0$ and is analytically continued for $\text{Im}(\xi) \leq 0$. There is a subtle distinction between defining $\xi := \omega / (\sqrt{2}k)$ and $\xi := \omega / (\sqrt{2}|k|)$. We adopt the latter definition because it allows the use of the plasma dispersion function $Z(\xi)$ as originally defined by Fried and Conte [42]. In contrast, the former definition requires a redefinition of $Z(\xi)$; see Hunana et al. [40, §2.2]. The asymptotic expansion of the response function is given by [40, §3]:

$$R(\xi) = 1 + i\sqrt{\pi}\xi - 2\xi^2 - i\sqrt{\pi}\xi^3 + \frac{4}{3}\xi^4 + i\frac{\sqrt{\pi}}{2}\xi^5 - \frac{8}{15}\xi^6 - i\frac{\sqrt{\pi}}{6}\xi^7 + \frac{16}{105}\xi^8 + \dots \quad \text{for} \quad |\xi| \ll 1, \quad (6)$$

$$R(\xi) = i\sigma\sqrt{\pi}\xi \exp(-\xi^2) - \frac{1}{2\xi^2} - \frac{3}{4\xi^4} - \frac{15}{8\xi^6} - \frac{105}{16\xi^8} - \frac{945}{32\xi^{10}} - \frac{10395}{64\xi^{12}} - \frac{135135}{128\xi^{14}} + \dots \quad \text{for} \quad |\xi| \gg 1, \quad (7)$$

where

$$\sigma = \begin{cases} 0 & \text{if } \text{Im}(\xi) > 0, \\ 1 & \text{if } \text{Im}(\xi) = 0, \\ 2 & \text{if } \text{Im}(\xi) < 0. \end{cases}$$

The response function captures key microscopic dynamics of the linear Vlasov-Poisson system, such as wave-particle resonance.

2.3. Asymmetrically Weighted Hermite Expansion

We discretize the electron distribution function in velocity space via an asymmetrically weighted (AW) Hermite spectral expansion, where the weight function does not equal unity. Hermite-based velocity discretizations inherently separate different scales (analogous to other orthogonal bases, e.g. Fourier), offering insight into the propagation of free energy (anisotropy or inhomogeneity in the initial distribution function) across scales in both linear and nonlinear processes [43]. Additionally, the AW Hermite expansion, in particular, conserves mass, momentum, and energy (if coupled with a conserving spatial and temporal integrator). The AW Hermite expansion is given by

$$\hat{f}(v) \approx \sum_{n=0}^{N_v-1} \hat{C}_n \psi_n(v) \quad \text{and} \quad f_0(v) = \frac{1}{\sqrt{2}} \psi_0(v), \quad (8)$$

where

$$\psi_n(v) := (\pi 2^n n!)^{-\frac{1}{2}} \mathcal{H}_n \left(\frac{v}{\sqrt{2}} \right) \exp \left(-\frac{v^2}{2} \right), \quad (9)$$

$$\psi^n(v) := (2^n n!)^{-\frac{1}{2}} \mathcal{H}_n \left(\frac{v}{\sqrt{2}} \right),$$

$$\mathcal{H}_n(v) := (-1)^n \exp(v^2) \frac{d^n}{dv^n} \exp(-v^2).$$

The limit relation of the AW Hermite basis function [44, §22.15] is given by

$$\lim_{n \rightarrow \infty} \psi_n(v) \propto \begin{cases} \cos(\sqrt{n}v) \exp\left(-\frac{v^2}{2}\right) & \text{if } n \text{ is even,} \\ \sin(\sqrt{n-1}v) \exp\left(-\frac{v^2}{2}\right) & \text{if } n \text{ is odd,} \end{cases} \quad (10)$$

such that the shortest wave-length λ_v in velocity space is resolved by the last Hermite basis of $N_v - 1$, i.e. $\lambda_v \approx 2\pi/\sqrt{N_v - 1}$. The orthogonality and recursive properties of the AW Hermite basis [44, §22.2–22.8] are

$$\int_{\mathbb{R}} \psi_n(v) \psi^m(v) dv = \sqrt{2} \delta_{n,m} \quad (11)$$

$$\frac{d\psi_n}{dv} = -\sqrt{n+1} \psi_{n+1}(v) \quad (12)$$

$$v\psi_n(v) = \sqrt{n+1} \psi_{n+1}(v) + \sqrt{n} \psi_{n-1}(v). \quad (13)$$

Inserting the spectral expansion in Eq. (8) in the linearized Vlasov equation (4) and employing the orthogonality in Eq. (11) and recursive properties in Eqns. (12)–(13) results in

$$-i\omega \hat{C}_n + \underbrace{ik \left(\sqrt{n+1} \hat{C}_{n+1} + \sqrt{n} \hat{C}_{n-1} \right)}_{\text{advection}} - \underbrace{\frac{ik\hat{\phi}}{\sqrt{2}} \delta_{n,1}}_{\text{acceleration}} = 0, \quad (14)$$

with the convention of $\hat{C}_{<0} = 0$ and the closure by truncation $\hat{C}_{N_v} = 0$, such that the closure term introduces an error only in the advection term $v\partial_x f$. We later consider other closure ideas in section 3.3. Then, in vector form, Eq. (14) becomes

$$\omega \bar{C} = k \bar{A} \bar{C} + k \hat{\phi} \bar{B} \quad \Rightarrow \quad \left(\xi \mathbb{I}_{N_v} - \frac{k}{\sqrt{2}|k|} \bar{A} \right) \bar{C} = \frac{k\hat{\phi}}{\sqrt{2}|k|} \bar{B}, \quad (15)$$

where $\bar{C} := [\hat{C}_0, \hat{C}_1, \hat{C}_2, \dots, \hat{C}_{N_v-1}]^\top \in \mathbb{R}^{N_v}$, $\bar{B} := [0 \ -\frac{1}{\sqrt{2}} \ 0 \ \dots \ 0]^\top \in \mathbb{R}^{N_v}$, $\mathbb{I}_{N_v} \in \mathbb{R}^{N_v \times N_v}$ is the identity matrix, the variable ξ is defined in Eq. (5), and

$$\bar{A} := \begin{bmatrix} 0 & \sqrt{1} & 0 & \dots & & \\ \sqrt{1} & 0 & \sqrt{2} & & & \\ 0 & \sqrt{2} & 0 & \sqrt{3} & & \\ & & & \ddots & & \\ \dots & 0 & \sqrt{N_v-2} & & 0 & \sqrt{N_v-1} \\ \dots & \dots & 0 & \sqrt{N_v-1} & 0 & 0 \end{bmatrix} \in \mathbb{R}^{N_v \times N_v}. \quad (16)$$

Therefore, inserting Eq. (15) in the response function definition in Eq. (5) results in the following Hermite approximation to the response function

$$\begin{aligned} R_{N_v}^{\text{aw}}(\xi) &:= \frac{\hat{n}}{\hat{\phi}} = \frac{\sqrt{2}\hat{C}_0}{\hat{\phi}} = \frac{\sqrt{2}}{\hat{\phi}} [1 \ 0 \ 0 \ \dots \ 0] \left(\xi \mathbb{I}_{N_v} - \frac{k}{\sqrt{2}|k|} \bar{A} \right)^{-1} \left(\frac{k\hat{\phi}}{\sqrt{2}|k|} \bar{B} \right) \\ &= \frac{-k}{\sqrt{2}|k|} [1 \ 0 \ 0 \ \dots \ 0] \left(\xi \mathbb{I}_{N_v} - \frac{k}{\sqrt{2}|k|} \bar{A} \right)^{-1} [0 \ 1 \ 0 \ \dots \ 0]^\top. \end{aligned} \quad (17)$$

We compute the response function symbolically, which limits the computation to a modest velocity resolution. For example, some analytical results are as follows

$$\begin{aligned} R_3^{\text{aw}}(\xi) &= \frac{-1}{2\xi^2 - 3}, \\ R_4^{\text{aw}}(\xi) &= \frac{3 - 2\xi^2}{4\xi^4 - 12\xi^2 + 3}, \\ R_5^{\text{aw}}(\xi) &= \frac{7 - 2\xi^2}{4\xi^4 - 20\xi^2 + 15}, \\ R_6^{\text{aw}}(\xi) &= \frac{-4\xi^4 + 24\xi^2 - 15}{8\xi^6 - 60\xi^4 + 90\xi^2 - 15}. \end{aligned}$$

The asymptotic results for $|\xi| \ll 1$ (Taylor/Maclaurin series) are

$$\begin{aligned} R_3^{\text{aw}}(\xi) &= \frac{1}{3} + \frac{2\xi^2}{9} + \frac{4\xi^4}{27} + \mathcal{O}(\xi^6), \\ R_4^{\text{aw}}(\xi) &= \boxed{1} + \frac{10\xi^2}{3} + 12\xi^4 + \mathcal{O}(\xi^6), \\ R_5^{\text{aw}}(\xi) &= \frac{7}{15} + \frac{22\xi^2}{45} + \frac{356\xi^4}{675} + \mathcal{O}(\xi^6), \\ R_6^{\text{aw}}(\xi) &= \boxed{1} + \frac{22\xi^2}{5} + \frac{68\xi^4}{3} + \mathcal{O}(\xi^6), \end{aligned}$$

and for $|\xi| \gg 1$ (Laurent series) are

$$\begin{aligned} R_3^{\text{aw}}(\xi) &= \boxed{-\frac{1}{2\xi^2} - \frac{3}{4\xi^4}} - \frac{9}{8\xi^6} + \mathcal{O}\left(\frac{1}{\xi^8}\right), \\ R_4^{\text{aw}}(\xi) &= \boxed{-\frac{1}{2\xi^2} - \frac{3}{4\xi^4} - \frac{15}{8\xi^6}} - \frac{81}{16\xi^8} + \mathcal{O}\left(\frac{1}{\xi^{10}}\right), \\ R_5^{\text{aw}}(\xi) &= \boxed{-\frac{1}{2\xi^2} - \frac{3}{4\xi^4} - \frac{15}{8\xi^6} - \frac{105}{16\xi^8}} - \frac{825}{32\xi^{10}} + \mathcal{O}\left(\frac{1}{\xi^{12}}\right), \\ R_6^{\text{aw}}(\xi) &= \boxed{-\frac{1}{2\xi^2} - \frac{3}{4\xi^4} - \frac{15}{8\xi^6} - \frac{105}{16\xi^8} - \frac{945}{32\xi^{10}}} - \frac{9675}{64\xi^{12}} + \mathcal{O}\left(\frac{1}{\xi^{14}}\right). \end{aligned}$$

The terms in the box above match the analytic response function coefficients at the respective asymptotic limit; see Eqns. (6)–(7).

The Hermite response function approximations have the correct asymptotic behavior in the fluid limit $|\xi| \gg 1$, i.e. when the phase velocity is much larger than the thermal velocity. In this region, increasing the number of moments improves the order of accuracy of the asymptotic expansion. However, in the adiabatic limit of $|\xi| \ll 1$, the accuracy of the approximation does not improve as we increase the number of Hermite moments N_v . Additionally, models with even N_v are more accurate in the $|\xi| \ll 1$ limit in comparison to models with odd N_v (at least to the zeroth order approximation) [45]. The mathematical reasoning is that the eigenvalues of the skew-symmetric advection matrix $ik\bar{A}$ defined in Eq. (16) are purely imaginary in the even-dimension case, whereas, in the odd-dimension case, there is an additional unpaired zero eigenvalue. Figure 1 shows the Hermite response function approximation for models with three to six moments. The Hermite approximations have purely

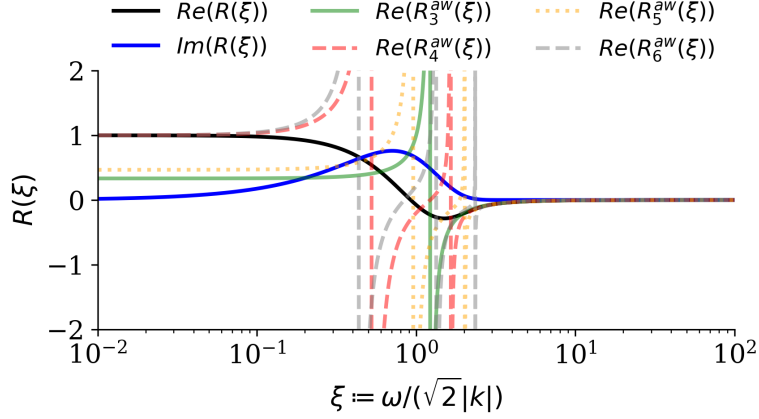


Figure 1: The collisionless Hermite response function approximation with closure by truncation and $N_v = 3, 4, 5, 6$. As expected, the approximations are most accurate in the high-phase velocity region $|\xi| \gg 1$ as there are weak kinetic effects in this region. In the small phase velocity region $|\xi| \ll 1$, the even N_v approximations are more accurate than the odd N_v approximations (up to the zeroth order approximation).

real poles in the $|\xi| \sim 1$ region that cause the response function to grow unbounded. Furthermore, the kinetic response function $R(\xi)$ has both real and imaginary components for purely real ξ , whereas the approximation $R_{N_v}^{\text{aw}}(\xi)$ is purely real for purely real ξ . A purely real response function indicates that the approximate discrete system cannot sustain a phase shift between the density and electrostatic potential perturbations.

3. Linear Spectral Deformation via Artificial Collisions, Filtering, and Nonlocal Closures

This section outlines three approaches for modifying the linearized spectral coefficient evolution equation (14) to accurately capture wave-particle resonance effects. These approaches comprise artificial collisions (section 3.1), filtering (section 3.2), and nonlocal closure (section 3.3). We compare the methods' ability to approximate the analytic linear response function in section 3.4 and the dispersion relation in section 3.5.

3.1. Artificial Collisions

Previous work by [1, 9, 15, 16, 22, 23, 46–49] include artificial collisions to introduce velocity-space dissipation, which allows the solvers to recover the Landau root [26] as a discrete eigenvalue of the discretized Vlasov-Poisson system. Hypercollisionality is similar in principle to hyperviscosity methods commonly used in spectral discretizations of hydrodynamic turbulence [25, 50], as both introduce higher-order dissipation to manage small-scale features and prevent unphysical recurrence or energy accumulation. Joyce et al. [7] introduce a hypercollisional operator based on powers of the LB [29] collisional operator, i.e.

$$\mathcal{C}_{\text{hyper}}(f) := \nu \mathcal{D}^{2\alpha-1} \tilde{\mathcal{D}}^{2\alpha-1} f \quad \text{with} \quad \mathcal{D}f := \frac{\partial}{\partial v} f, \quad \tilde{\mathcal{D}}f := \left(\frac{\partial}{\partial v} + v \right) f, \quad \mathcal{C}_{\text{hyper}}(f_0) = 0, \quad (18)$$

where $\nu \in \mathbb{R}_+$ is the normalized collisional frequency and $\alpha \in \mathbb{N}_{\geq 1}$ controls the order of dissipation. The artificial collision operator is added to the right-hand side of Eq. (1). If $\alpha \geq 2$, the hypercollisional operator conserves mass, momentum, and energy [51]. The Hermite basis function $\psi_n(v)$ defined in Eq. (9) is an eigenfunction of the collisional operator with eigenvalue $-\nu n!/(n-2\alpha+1)!$. The operator in Eq. (18) recovers the LB [29] collisional operator when $\alpha = 1$. Similarly, Camporeale et al. [23] adopted a hypercollisional operator that corresponds to the operator in Eq. (18) with $\alpha = 2$ (up to a normalizing factor), which was adopted in various studies, e.g. [11–13, 15–17]. Following the recursive Hermite properties in Eq. (12)–(13), see Funaro and Manzini [51], the normalized artificial collisions operator in Hermite space acts as

$$\mathcal{C}_{\text{hyper}}(\hat{C}_n) = -\underbrace{\nu \frac{n!}{(n-2\alpha+1)!}}_{\text{damping rate } \propto n^{2\alpha-1}} \underbrace{\frac{(N_v-2\alpha)!}{(N_v-1)!}}_{\text{normalizing factor}} \hat{C}_n \quad (19)$$

such that the last Hermite moment \hat{C}_{N_v-1} damping rate is $\nu \in \mathbb{R}_+$. The hypercollisional operator should always be applied in a convergence sense, ensuring that it does not substantially alter the collisionless physics of interest. An important feature of the operator is that the damping rate increases with larger n Hermite coefficients, scaling as $n^{2\alpha-1}$.

3.2. Filtering

The low-pass exponential filter introduced in Cai and Wang [33] for the Hermite system, based on Hou and Li [31] filter, modifies the Hermite moments as follows

$$C_n \rightarrow C_n \sigma \left(\frac{n}{N_v - 1} \right) \quad \text{and} \quad \sigma \left(\frac{n}{N_v - 1} \right) := \exp \left(-\chi \left(\frac{n}{N_v - 1} \right)^p \right).$$

This filter corresponds to computing the solution to the modified equation, where the following term is added to the right-hand side of the Vlasov equation (1):

$$\mathcal{C}_{\text{HouLi}}(f) = \chi \frac{(-1)^{p+1}}{\Delta t (N_v - 1)^p} \hat{\mathcal{D}}^p f, \quad \text{with} \quad \hat{\mathcal{D}} f := \frac{\partial}{\partial v} \left[\exp \left(-\frac{v^2}{2} \right) \frac{\partial}{\partial v} \left(\exp \left(\frac{v^2}{2} \right) f \right) \right], \quad \mathcal{C}_{\text{HouLi}}(f_0) = 0,$$

where $\Delta t \in \mathbb{R}_{>0}$ is the time step, and $\chi \in \mathbb{R}$ and $p \in \mathbb{N}_{>0}$ are tunable parameters of the exponential filter. Following the recursive Hermite properties in Eq. (12)–(13), the filtering operator in Hermite space acts as

$$\mathcal{C}_{\text{HouLi}}(\hat{C}_n) = -\underbrace{\frac{\chi}{\Delta t} \left(\frac{n}{N_v - 1} \right)^p}_{\text{damping rate } \propto n^p} \hat{C}_n. \quad (20)$$

Hou and Li [31] use $p = 36$ for spatial Fourier smoothing in hydrodynamic simulations, a parameter later adopted for AW Hermite-based solvers (see, e.g., [33, 34, 43, 47, 52]). In this paper, we adopt the same scaling $p = 36$. We note that filtering and artificial collisions are fundamentally equivalent methods in the sense that a combination of parameters can be found so that both methods yield very similar damping rates. This is demonstrated in Fig. 2. Specifically, for $N_v = 20$, artificial collisions with $\alpha = 8$ have a damping rate comparable to that of filtering. When $N_v = 10^3$, artificial collisions with $\alpha = 18$ show a damping rate similar to that of filtering. In Appendix A, we discuss another commonly used filter developed by Klimas [30]. The Klimas filter does not correspond to a true velocity space dissipation and hence the Landau root is not a discrete mode of the Klimas filtered AW Hermite discretization with closure by truncation.

3.3. Hermite Hammett-Perkins Nonlocal Linear Closures

Hammett and Perkins [36] developed a nonlocal linear closure that accounts for collisionless Landau damping effects in a fluid model. This closure approximates the highest moment in the fluid hierarchy by a linear combination of lower-order moments in Fourier space. The transformation between Hermite moments and fluid moments is nonlinear and invertible, such that a linear fluid moment closure corresponds to a nonlinear Hermite moment closure, and *vice versa* [38, §3]. The transformation from fluid moments to Hermite moments is

$$\begin{aligned} \hat{n} = \sqrt{2}\hat{C}_0 &\implies \hat{C}_0 = \frac{\hat{n}}{\sqrt{2}} \\ \hat{u} = \frac{\hat{C}_1}{\hat{C}_0} &\implies \hat{C}_1 = \frac{\hat{u}\hat{n}}{\sqrt{2}} \\ \hat{p} = 2\hat{C}_2 + \sqrt{2}\hat{C}_0 - \frac{\sqrt{2}\hat{C}_1^2}{\hat{C}_0} &\implies \hat{C}_2 = \frac{\hat{p} - \hat{n} + \hat{u}^2\hat{n}}{2} \\ \hat{q} = 2\sqrt{3}\hat{C}_3 - \frac{6\hat{C}_2\hat{C}_1}{\hat{C}_0} + \frac{2\sqrt{2}\hat{C}_1^3}{\hat{C}_0^2} &\implies \hat{C}_3 = \frac{\hat{q} + 3\hat{u}(\hat{p} - \hat{n}) + \hat{u}^3\hat{n}}{2\sqrt{3}} \end{aligned}$$

where the first four fluid moments are density \hat{n} , bulk velocity \hat{u} , pressure \hat{p} , and heat flux \hat{q} :

$$\hat{n} := \int_{\mathbb{R}} \hat{f}(v) dv, \quad \hat{n}\hat{u} := \int_{\mathbb{R}} v \hat{f}(v) dv, \quad \hat{p} := \int_{\mathbb{R}} (v - \hat{u})^2 \hat{f}(v) dv, \quad \hat{q} := \int_{\mathbb{R}} (v - \hat{u})^3 \hat{f}(v) dv.$$

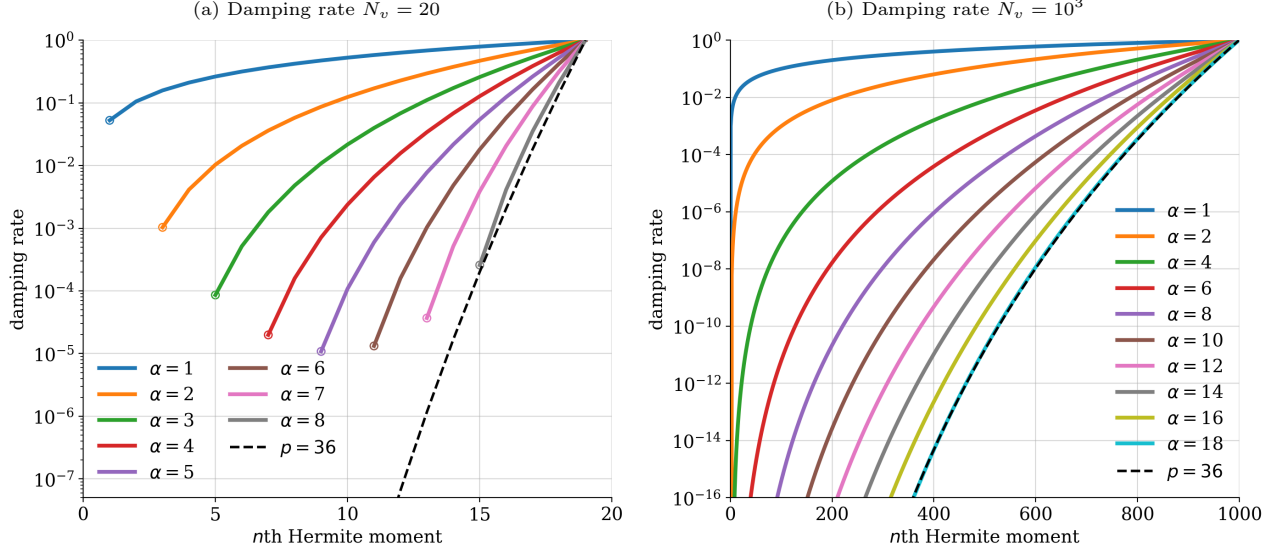


Figure 2: Damping rates for artificial collisions at various values of α (solid lines), as described in Eq. (19), compared to the filtering approach with $p = 36$ (dashed line), as outlined in Eq. (20). For $N_v = 20$, corresponding to subfigure (a), artificial collisions with $\alpha = 8$ produce a damping rate comparable to filtering. Similarly, for $N_v = 10^3$, corresponding to subfigure (b), artificial collisions with $\alpha = 18$ yield a damping rate similar to filtering.

Hammett and Perkins [36] derived a closure for three- and four-moment fluid models, e.g. the three-moment closure relates the heat flux to the pressure and density as follows:

$$\hat{q} = -i \frac{2\sqrt{2}}{\sqrt{\pi}} \frac{k}{|k|} (\hat{p} - \hat{n}).$$

In Hermite space, this leads to a nonlinear closure expressed as $\hat{C}_3 = \mathcal{F}(\hat{C}_2, \hat{C}_1, \hat{C}_0)$. By neglecting quadratic and higher-order perturbations, the first-order approximation yields the following closure

$$\hat{C}_3 = -i \frac{2\sqrt{2}}{\sqrt{3\pi}} \frac{k}{|k|} \hat{C}_2.$$

Following the work by Hammett et al. [24], Smith [38], we generalize the mathematical approach to higher N_v dimensions for a nonlocal linear closure of the form

$$\hat{C}_{N_v} = \sum_{n=N_v-N_m}^{N_v-1} i\mu_n \frac{k}{|k|} \hat{C}_n. \quad (21)$$

The number of lower order Hermite moments used to close the equations, which corresponds to the number of adjustable parameters in the linear closure, is denoted by $N_m \in \mathbb{N}_{>0}$. The linear closure coefficients $\mu_n \in \mathbb{C}$ are chosen by matching the approximate response function to the analytic response function at the asymptotic limit of $|\xi| \ll 1$, see Eq. (6). The linear closure retains the same order of accuracy at the fluid limit $\xi \gg 1$ as the closure by truncation. Since we solve for the approximate response function symbolically, computational limitations require keeping N_m relatively small. To the best of our knowledge, this study is the first to interpret the nonlocal closure approach as a method to mitigate recurrence and suppress filamentation artifacts in kinetic simulations. The concept of nonlocal Hermite closure is similar to the approach proposed by Eliasson [53], which introduced absorbing velocity boundary conditions in Fourier velocity discretizations to reduce recurrence effects.

The closure is nonlocal in space, since for example the term $ik/|k|g(k)$ in configuration space becomes $\int_0^\ell [g(x+y) - g(x-y)]/y dy$, where $g(x)$ is an arbitrary function and $x \in [0, \ell]$. For practical computational purposes, local (e.g. finite-difference) numerical solvers can approximate the nonlocal closure as a sum of Lorentzians in Fourier space which solves a modified Helmholtz equation in configuration space x , see Dimits et al. [54] for more details.

Table 1: The optimal tunable parameter of each method based on matching the asymptotic limit $\xi \ll 1$ (adiabatic limit). The three methods are artificial collisions in Eq. (19), nonlocal closure in Eq. (21), and filtering in Eq. (20).

N_v	collisions $\alpha = 1$ ν	collisions $\alpha = 2$ ν	collisions $\alpha = 3$ ν	collisions $\alpha = 4$ ν	nonlocal closure $N_m = 1$ μ_{N_v-1}	nonlocal closure $N_m = 3$ $\mu_{N_v-1}, \mu_{N_v-2}, \mu_{N_v-3}$	filtering $\chi/\Delta t$
4	1.69	1.88	X	X	-0.93	-1.31, 0, -0.30	1.88
6	1.74	9.69	2.35	X	-0.96	-1.37, 0, -0.37	2.35
8	1.72	17.65	4.81	2.74	-0.97	-1.40, 0, -0.40	2.75
10	1.68	6.46	13.31	11.19	-0.97	-1.42, 0, -0.42	3.13
12	1.64	6.63	19.83	24.51	-0.98	-1.44, 0, -0.44	3.51

3.4. Linear Response Function Approximation

The procedure to derive the approximate response function with artificial collisions, filtering, or a nonlocal closure approach follows the same formula as Eq. (17). The only difference is in the advection matrix $\bar{A} \in \mathbb{C}^{N_v \times N_v}$ which is defined in Eq. (16). For artificial collisions and filtering, the diagonal elements of the advection matrix are adjusted to match the corresponding dissipation operator. For the nonlocal closure, modifications are made to the entries in the last row of the advection matrix.

The convergence rates of the different methods are shown in Figure 3a. The absolute error of the response function is evaluated using the L_2 norm on a log-uniform grid of $\xi \in [10^{-2}, 10^2]$ with 10^5 nodes (more nodes do not change the error significantly). The absolute error is plotted with the optimal tunable parameter of the method, such that the approximate response function matches the analytic response at the asymptotic limit of $|\xi| \ll 1$. We indicate the optimal parameters for each method in Table 1. For artificial collisions, the tunable parameter is the artificial collisional rate $\nu \in \mathbb{R}_+$ in Eq. (19). For the nonlocal closure with $N_m = 1$, the tunable parameter is the coefficient in the linear relation $\mu_n \in \mathbb{C}$ in Eq. (21). For filtering, the tunable parameter is $\chi/\Delta t \in \mathbb{R}_+$ in Eq. (20). There is not a clear trend in optimal parameter variation as a function of the velocity resolution N_v . Interestingly, the optimal closure coefficients with $N_m = 3$, show that $\mu_{N_v-2} = 0$ for all considered even N_v , such that a nonlocal closure with $N_m = 2$ and $N_m = 1$ are equivalent. The approximate response function for both artificial collisions and filtering depends on the wavenumber k , i.e. $R_{N_v}^{qu}(\xi, k)$. We present the results with $k = 1$, and additional tests (not shown here) indicate that varying k does not significantly influence the convergence or accuracy of the methods. The most accurate methods are hypercollisions with $\alpha = 2$ and $\alpha = 3$. The hypercollisional operator with $\alpha = 2$ converges about four times faster than that with $\alpha = 1$ (LB collisions). Accuracy decreases when $\alpha = 4$, indicating that $\alpha = 2$ and $\alpha = 3$ represent the optimal range for the order of artificial collisions. Additionally, the nonlocal closure method with $N_m = 3$ converges approximately twice as fast as with $N_m = 1$. As shown by Smith [38], the convergence rate of the nonlocal closure improves as N_m increases. However, matching the closure coefficient becomes increasingly difficult as N_m and N_v increase since calculating the approximate response function requires a symbolic matrix inversion, see Eq. (17), with N_m nonlinear solves to match to the asymptotic limit. The filtering approximation converges slowly, similar to the nonlocal closure method with $N_m = 1$.

Figure 3b shows the absolute error of the approximate response function for $N_v = 12$. In all cases, the largest error occurs in the wave-particle resonance region $\xi \sim 1$. However, these approximations show a significant improvement compared to closure by truncation without dissipation, as shown in Figure 1. In all approximations, the response function poles are complex, resulting in damping. For artificial collisions, the results with $\alpha = 2$ and $\alpha = 3$ are most accurate at the wave-particle resonance region $\xi \sim 1$. For nonlocal closures, as expected, increasing N_m , i.e., the number of coefficients matched in the limit of $|\xi| \ll 1$, improves the accuracy of the response function. Lastly, the filtering approximation error is similar to the nonlocal closure method with $N_m = 1$. Overall, given the constraints on the nonlocal closure method parameter N_m imposed by symbolic computation limitations, hypercollisions with $\alpha = 2$ or $\alpha = 3$ converge the fastest and are the most accurate approaches for approximating the response function under limited velocity resolution.

3.5. Linear Eigenvalue Analysis

The previous section focused on analyzing the behavior of the response function for the Vlasov equation alone. We now investigate the ability of the discrete models to replicate the dynamics of the linearized Vlasov-Poisson system, using the Landau damping problem as a test case. We set $\ell = 4\pi$ such that wavenumber k are

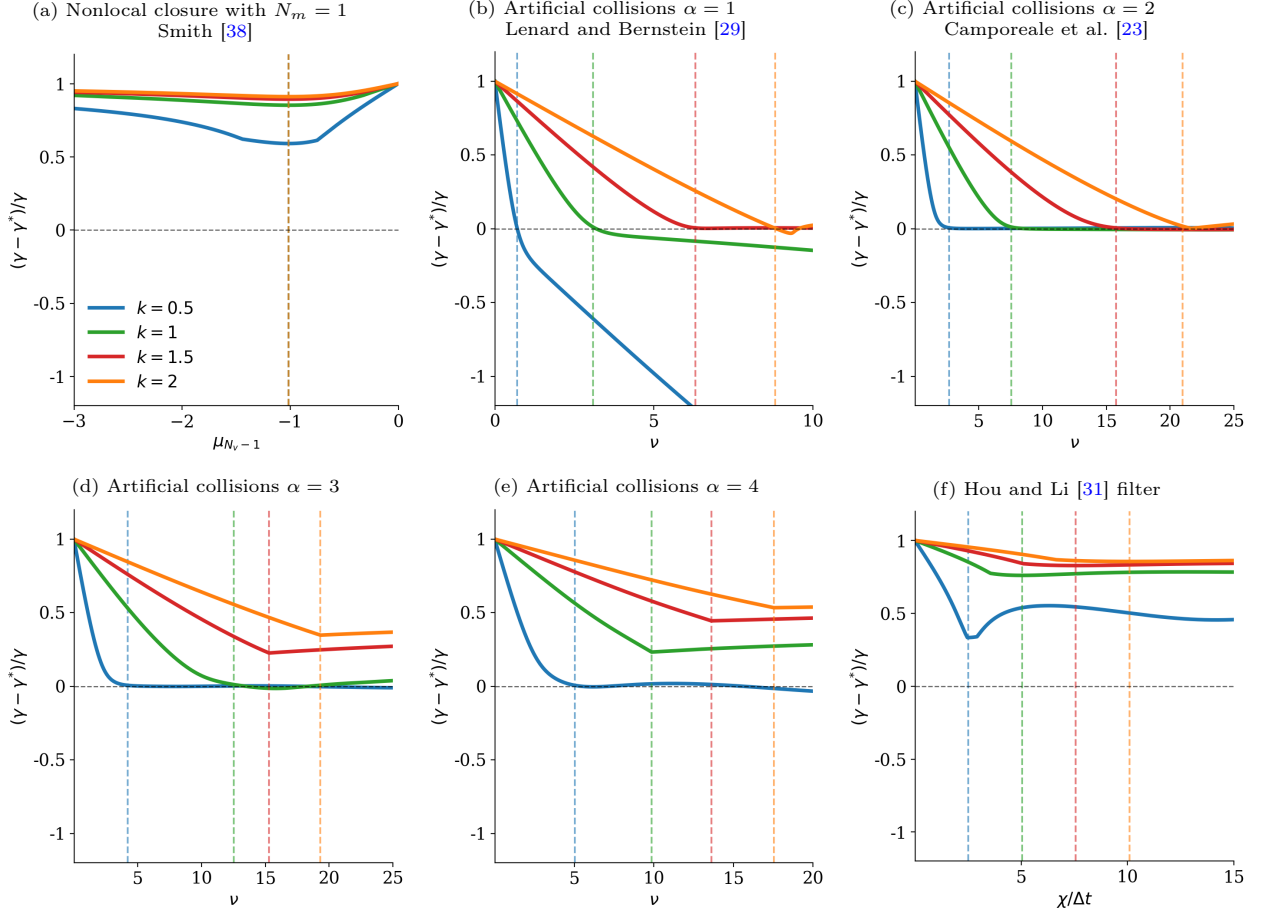


Figure 4: The relative error between the discrete system damping rate γ^* and the analytic damping rate γ for various spatial wavenumber $k \in \{0.5, 1, 1.5, 2\}$ with $N_v = 20$. Positive values lead to underdamping of the modes, while negative values correspond to overdamping. When the free parameters of the methods are set to zero, we recover the collisionless with closure by truncation approximation which incorrectly predicts $\gamma^* = 0$. Dashed vertical lines illustrate the optimal free parameter for each mode. The results show that only artificial collisions with $\alpha = 2$ can recover the correct damping rate across a range of wavenumbers.

velocity resolution increases. The artificial collision operator with $\alpha = \{3, 4\}$ no longer underdamps the larger wavenumber modes. Therefore, with sufficiently high-velocity resolution ($N_v > 100$), artificial collisions with $\alpha \in \{3, 4\}$ can accurately recover the correct Landau damping rate across a range of wavenumbers. However, in multidimensional simulations where computational limitations constrain velocity resolution, the artificial collision operator with $\alpha = 2$ remains the most effective choice, as demonstrated in Figure 4.

4. Numerical Results

We use the AW Hermite discretization in velocity and Fourier discretization in space, as described in Camporeale et al. [23], to simulate Landau damping with artificial collisions, filtering, and nonlocal closure approaches discussed in section 3. The linear and nonlinear Landau damping tests are initialized by perturbing the initial electron distribution function as follows

$$f(x, v, t = 0) = \frac{1 + \epsilon \sum_k \cos(kx)}{\sqrt{2\pi}} \exp\left(-\frac{v^2}{2}\right), \quad (22)$$

where ϵ is the perturbation amplitude. We set the spatial length to $\ell = 4\pi$, such that wavenumbers k are integer multiples of $1/2$. We use the second-order implicit midpoint integrator with the unpreconditioned Jacobian-Free-Newton-Krylov method with absolute and relative error set to 10^{-10} [55]. The time step is $\Delta t = 10^{-2}$ and the number of Fourier spectral terms in space is $N_x = 10$ for linear Landau damping in section 4.1 and

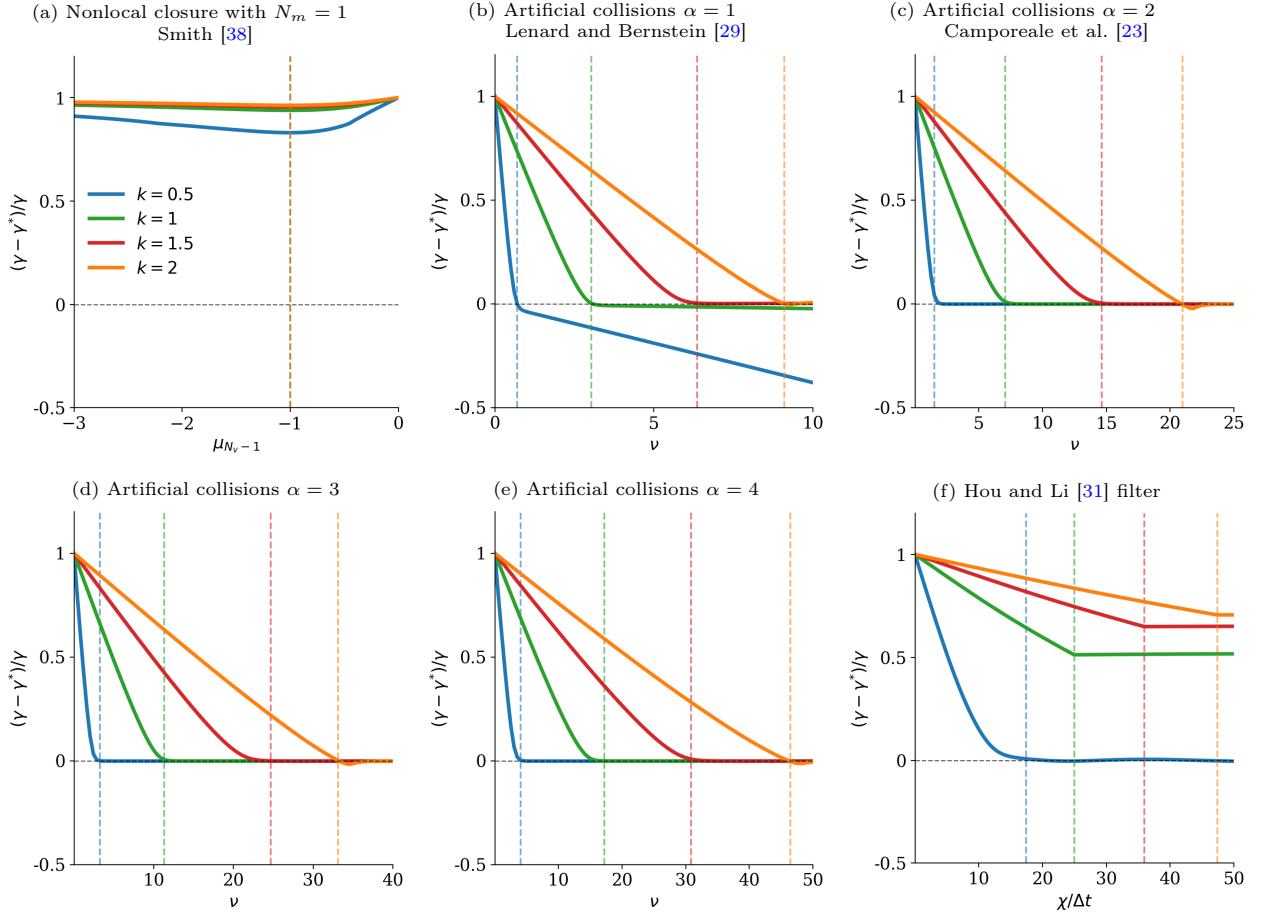


Figure 5: Same as Figure 4 with $N_v = 100$. In comparison to $N_v = 20$ in Figure 4, artificial collisions with $\alpha \in \{3, 4\}$ in subfigures (d)–(e) no longer underdamp the higher wavenumber modes. Artificial collisions with $\alpha = 1$ continue to overdamp smaller wavenumber modes. Nonlocal closure and filtering approaches continue to underdamp most (or all) modes.

Table 2: The optimal tunable parameter of each method based on minimizing the damping rate error for the highest wavenumber excited. The three methods are artificial collisions in Eq. (19), filtering in Eq. (20), and nonlocal closure in Eq. (21). The linear Landau damping parameters in section 4.1 are optimized with $N_v = 20$ and $k = 1.5$ and the nonlinear Landau damping parameters in section 4.2 are optimized with $N_v = 300$ and $k = 0.5$.

	collisions $\alpha = 1$ ν	collisions $\alpha = 2$ ν	collisions $\alpha = 3$ ν	filtering $\chi/\Delta t$	nonlocal closure $N_m = 1$ μ_{N_v-1}
linear Landau damping in section 4.1	6.30	16.76	15.29	7.56	-1.01
nonlinear Landau damping in section 4.2	0.55	1.31	2.01	12.23	-1.00

$N_x = 100$ for nonlinear Landau damping in section 4.2. The optimal tuning parameter of each method for the linear and nonlinear Landau tests are listed in Table 2, where the optimal parameters minimize the damping error via the eigenvalue analysis in section 3.5.

4.1. Linear Landau Damping

We investigate the impact of artificial collisions, filtering, and nonlocal closure approaches on the recurrence problem in linear Landau damping with $N_v = 20$. Table 2 lists the optimal tunable parameters for each method, which are derived through the eigenvalue analysis in section 3.5. Initially, two modes with $k = 0.5$ and $k = 1.5$ are perturbed with amplitude $\epsilon = 10^{-2}$ in Eq. (22). The velocity space Hermite moment cascade is shown in Figure 6. We plot the squared normalized magnitude of the Hermite coefficients with $k = 0.5$, more specifically $|\hat{C}_n(k = 0.5, t)|^2 / \max_n(|\hat{C}_n(k = 0.5, t)|^2)$. The results show transport from the zeroth to the highest order Hermite mode, which for the collisionless, nonlocal closure, and filtering, gets reflected from the finite Hermite resolution and backpropagates. For the linear Landau damping problem, Hermite flux only propagates from the lower to higher order Hermite modes as shown in Figure 6a for the collisionless simulation with closure by truncation and $N_v = 1,024$, and explained in greater detail in Parker and Dellar [43]. This backpropagation then artificially amplifies the zeroth order Hermite mode, resulting in a growth of the electric field. Artificial collisions suppress higher-order Hermite modes and prevent artificial backpropagation of Hermite flux.

Figure 7 shows the damping rate of the electric field. The closure by truncation without artificial collisions exhibits recurrence effects, with a recurrence period given by $T_{\text{rec}}(k) \approx \sqrt{N_v}/k$, such that $T_{\text{rec}}(k = 1.5) \approx 4$ and $T_{\text{rec}}(k = 0.5) \approx 13$. The nonlocal closure with one tunable parameter and filtering results also show recurrence effects and underestimate the damping rate, especially for $k = 1.5$. The recurrence period is slightly delayed in both approaches for $k = 0.5$, compared to the collisionless case with closure by truncation. Additionally, although the LB operator (i.e. artificial collisions with $\alpha = 1$) eliminates recurrence, it overdamps the $k = 0.5$ wave. This is expected since we chose to match the optimal free parameter ν to recover the correct damping rate for $k = 1.5$ wave; otherwise, if we chose the optimal ν to recover the correct damping rate for $k = 0.5$ mode, we would underdamp the $k = 1.5$ mode. Similarly, artificial collisions with $\alpha = 3$ eliminate recurrence but underdamp the $k = 1.5$ wave. These results confirm the findings from section 3.5, with artificial collisions with $\alpha = 2$ proving to be the most effective method for capturing the correct linear Landau damping phenomena for a range of wavenumbers in limited velocity resolution.

4.2. Nonlinear Landau Damping

For nonlinear Landau damping, we set the initial perturbation with wavenumber $k = 0.5$ and amplitude $\epsilon = 0.5$ in Eq. (22). The tunable parameters for each method are listed in Table 2 and are determined through the eigenvalue analysis in section 3.5 with $N_v = 300$, which aims to minimize errors in the linear theory damping rate. Parker and Dellar [43] describe the nonlinear Landau damping dynamics in terms of Hermite flux, where the initial linear decay phase of the electric field corresponds to forward-propagating Hermite modes. The subsequent growth phase is associated with backward-propagating Hermite modes. Eventually, a balance is reached between the forward and backward Hermite fluxes, leading to the nonlinear saturation phase. Therefore, the method's suppression of recurrence is more subtle in the nonlinear case since the goal is to suppress artificial backpropagation stemming from the finite resolution while permitting physical backpropagation caused by the nonlinear dynamics. Figure 8 shows the squared normalized magnitude of the Hermite coefficients with $k = 0.5$ (similar to Figure 6 for linear Landau damping). The results indicate that LB collisions, i.e. artificial collisions with $\alpha = 1$, prevent the backpropagation of Hermite flux from higher to lower Hermite coefficients.

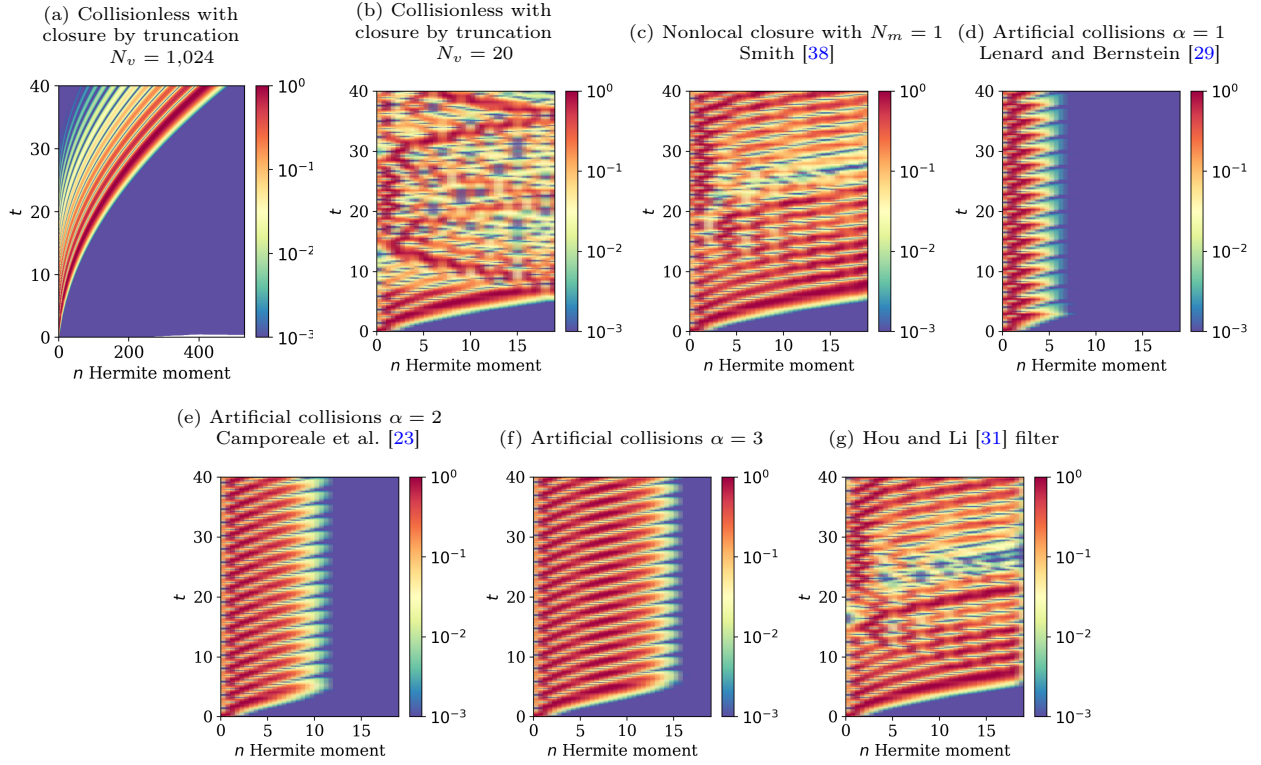


Figure 6: The squared normalized magnitude of the Hermite coefficients with $k = 0.5$ for (a) $N_v = 1,024$ and (b)-(g) $N_v = 20$. The results indicate that artificial collisions in subfigures (d)–(f) effectively mitigate recurrence caused by an artificial backpropagating Hermite cascade due to truncation, whereas nonlocal closure in subfigure (c) and filtering in subfigure (g) do not adequately suppress this backpropagation.

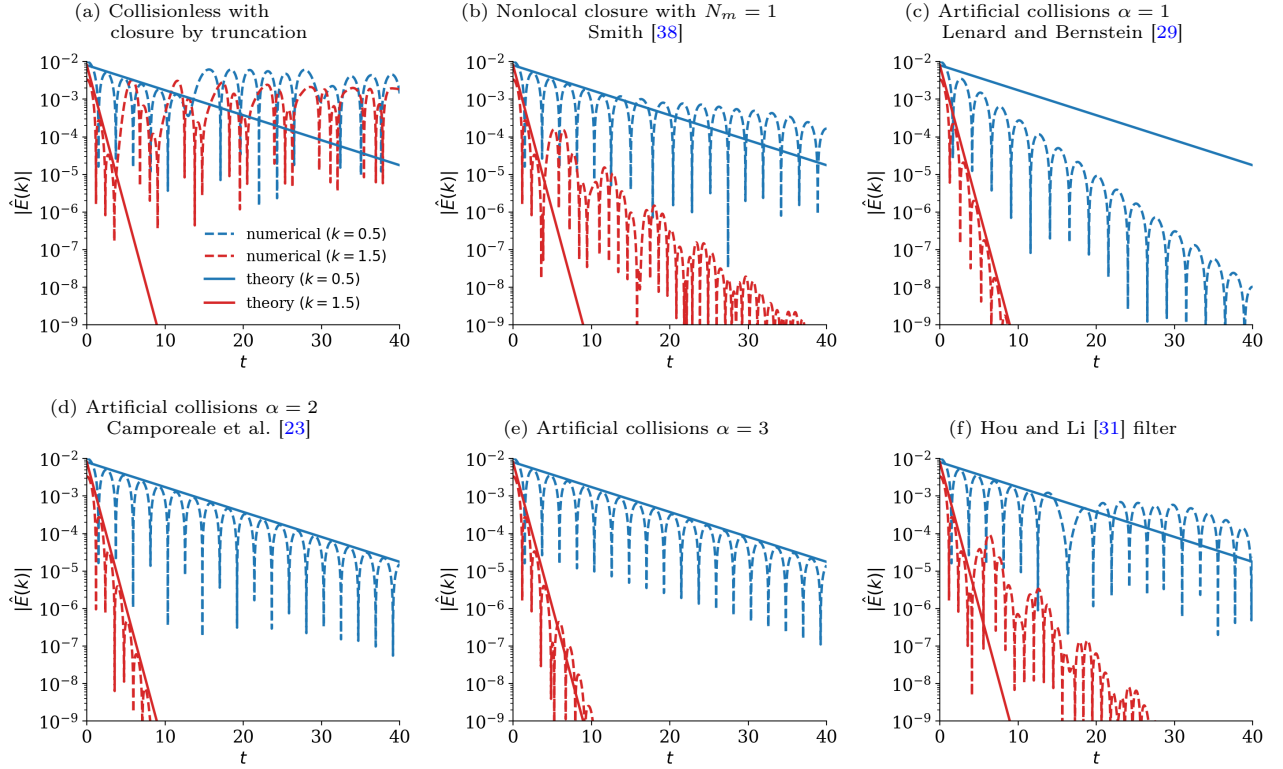


Figure 7: The linear Landau damping electric field Fourier coefficient magnitude of $k \in \{0.5, 1.5\}$ with $N_v = 20$. The solid lines show the analytic damping rate obtained from linear theory, i.e. solving $k^2 = -R(\xi)$. Recurrence time is given by $T_{\text{rec}}(k) \approx \sqrt{N_v}/k$, such that recurrence occurs at $T_{\text{rec}}(k = 1.5) \approx 4$ and $T_{\text{rec}}(k = 0.5) \approx 13$, as shown in subfigure (a). The numerical results show that only artificial collisions with $\alpha = 2$ in subfigure (c) can mitigate recurrence without overdamping the smallest wavenumber perturbations or underdamping the largest wavenumber perturbations.

Hypercollisions and filtering permit backpropagation while significantly damping the highest Hermite modes. Conversely, the nonlocal closure allows the distribution function to spread across all velocity scales including the highest Hermite mode.

Figure 9 compares the magnitude of the electric field second Fourier mode (i.e. $k = 1$) of the different methods against the reference solution obtained by a high-resolution dissipationless second-order central finite difference scheme presented in Shiroto et al. [56] with grid resolution $N_x = N_v = 16,384$. The electric field dynamics for the nonlocal closure, filtering, and higher-order artificial collisions ($\alpha \geq 2$) are similar, as both permit the backpropagation of Hermite flux, leading to the correct qualitative behavior of nonlinear saturation. In contrast, the LB operator, i.e. artificial collisions with $\alpha = 1$, entirely suppresses the backpropagation of Hermite flux, which overdamps the dynamics and incorrectly drives the system to thermal equilibrium. The LB results shown here are consistent with the previous analysis by Pezzi et al. [20]. Moreover, as expected, the collisionless case with closure by truncation exhibits recurrence, leading to incorrect growth in the electric field.

The electron distribution function in phase space is shown in Figure 10, which becomes highly oscillatory due to filamentation in velocity space. The oscillations then roll up to form a vortex centered at the phase speed $\omega_r/k = \pm 2.8$. The velocity resolution of $N_v = 300$ does not resolve the filamentation microstructures at $t = 40$ by comparison to the reference solution in Figure 10g, yet all methods besides LB collisions capture the correct particle trapping vortex around the phase speed. At $t = 40$, the shortest velocity wavelength of the filaments in the reference solution is $\lambda_v \approx 0.01$. According to Eq. (10), resolving such velocity scales with the Hermite discretization requires $N_v \approx (2\pi/\lambda_v)^2 = 394,784$. The phase space dynamics are distorted by numerical filamentation artifacts in the collisionless case with closure by truncation. The filamentation artifacts shown at $t = 40$ for the nonlocal closure and filtering approaches are a result of limited velocity resolution. The hypercollisions simulation with $\alpha \geq 2$ smooths out any strong deformations of the particle distribution function while maintaining the correct plasma dynamics characteristics. Additionally, Figure 11 shows a cross-section of the electron distribution function at $t = 40$ and $x = 3\pi$, highlighting that artificial collisions are more effective in preserving the positivity of the electron distribution function compared to nonlocal closure and filtering techniques. In the spectral solver, the particle distribution function is not guaranteed to remain positive due to the orthogonal nature of the velocity basis functions, potentially leading to unphysical solutions. To enforce positivity, a square-root formulation can be used; see the work by Issan et al. [10], which employs this transformation for the symmetrically weighted Hermite discretization. Pagliantini et al. [12] showed that positivity can be improved by dynamically adjusting the Hermite tunable parameters over time or increasing the artificial collisional frequency ν in Eq. (19) with $\alpha = 2$. This implies that the loss of positivity arises from insufficient spectral resolution. It is worth noting that even the reference solution exhibits negativity near $v \approx 2.5$, as the finite difference scheme does not enforce positivity.

5. Conclusions

This study evaluated the effectiveness of artificial collisions, filtering, and nonlocal closure methods in mitigating filamentation and recurrence artifacts in Hermite-based Vlasov-Poisson simulations. Our analysis, including comparisons of linear kinetic response function, dispersion relation, and nonlinear simulation, indicates that higher-power artificial collisions (hypercollisions) provide the most robust solution for approximating correct Landau damping rates across a broad range of wavenumbers, particularly in multidimensional simulations constrained by limited velocity resolution. Filtering and nonlocal closures underestimate the damping rates, particularly at high wavenumber modes. In the nonlinear simulations, both hypercollisions, nonlocal closures, and Hou-Li filtering approximately distinguish between backward-propagating Hermite flux stemming from the nonlinear term and the finite truncation and mainly damp the latter. The LB collisional operators, on the other hand, completely prevent backward flux propagation from higher to lower Hermite modes.

The analysis highlights hypercollisions as a practical approach for enhancing accuracy in kinetic plasma simulations, as they effectively suppress artificial recurrence without compromising the accurate representation of collisionless dynamics. Future research could explore extending these methods to electromagnetic Vlasov-Maxwell simulations, including deriving nonlocal closures in Hermite space that capture electromagnetic wave-particle interaction such as cyclotron resonance similar to the four-moment fluid model in Jikei and Amano [57] but generalized to higher-moment models in Hermite space. Additionally, it would be interesting to examine a hybrid formulation of the different methods, e.g. nonlocal closure method coupled with filtering or artificial collisions. Lastly, future work could explore the response function approximation for non-Maxwellian equilibrium distributions [58], such as Kappa or Cauchy distributions with suprathermal tails [59]. For these non-Maxwellian

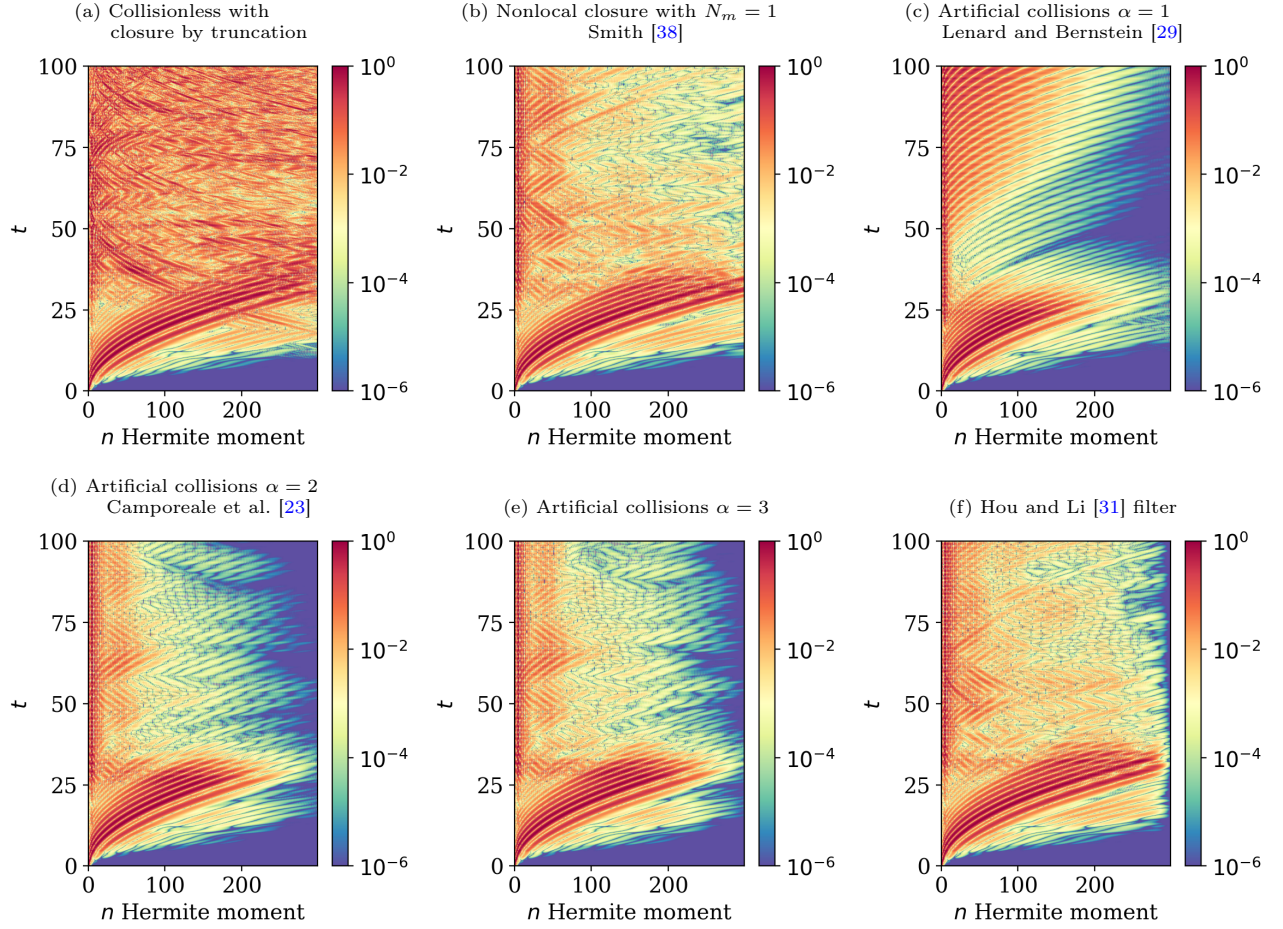


Figure 8: Same as Figure 6 for nonlinear Landau damping with $N_v = 300$. The nonlinear dynamics lead to the backward propagation of Hermite flux from higher to lower moments. Moreover, the finite dimensionality in velocity space introduces an artificial backward propagation of Hermite flux. The results from the nonlocal closure in subfigure (b) show that the method mitigates some of this backward propagation compared to subfigure (a). Artificial collisions in subfigures (c)–(e) and filtering in subfigure (f) significantly damp the highest modes.

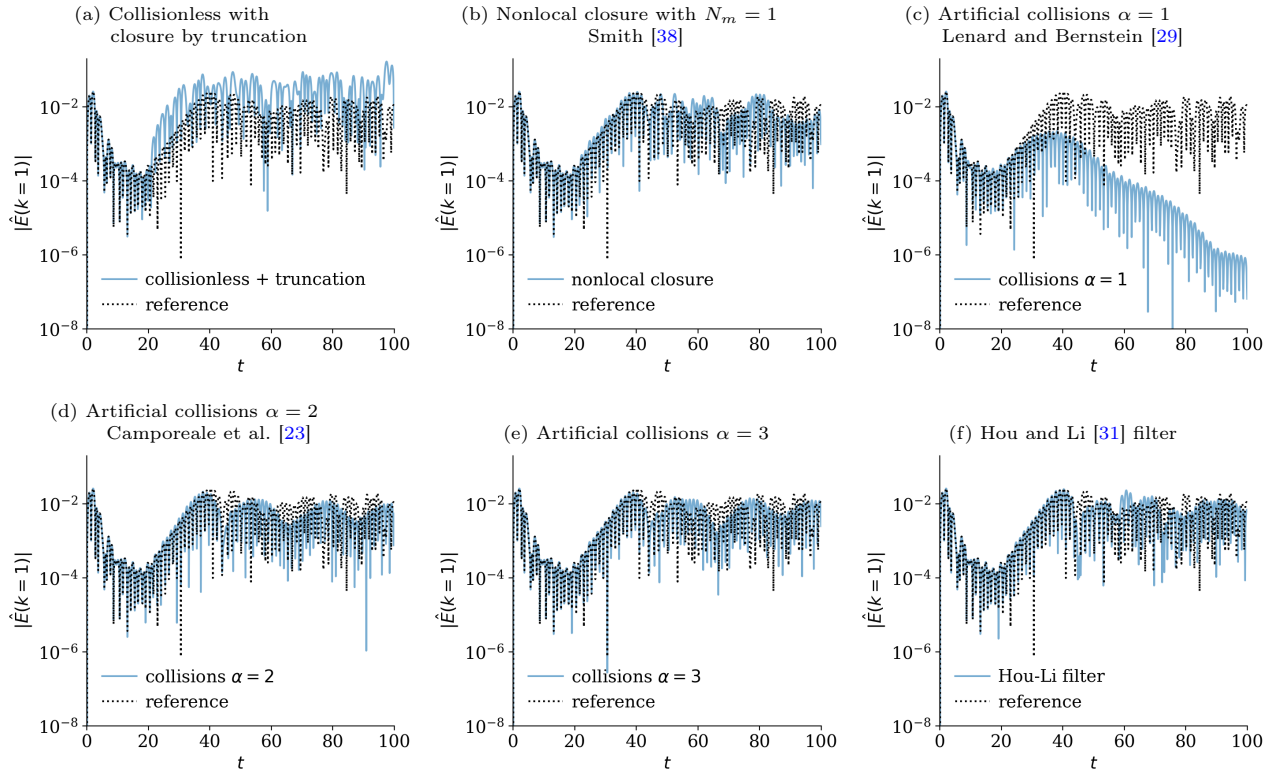


Figure 9: A comparison of the methods estimating the magnitude of the second Fourier mode of the electric field (i.e., $k = 1$) in nonlinear Landau damping for $N_v = 300$ against a high-resolution reference solution. In subfigure (c), the LB operator significantly alters the system’s dynamics, driving the plasma toward thermodynamic equilibrium. In contrast, all other methods in subfigures (b) and (d)–(f) qualitatively capture the collisionless dynamics during the saturation phase.

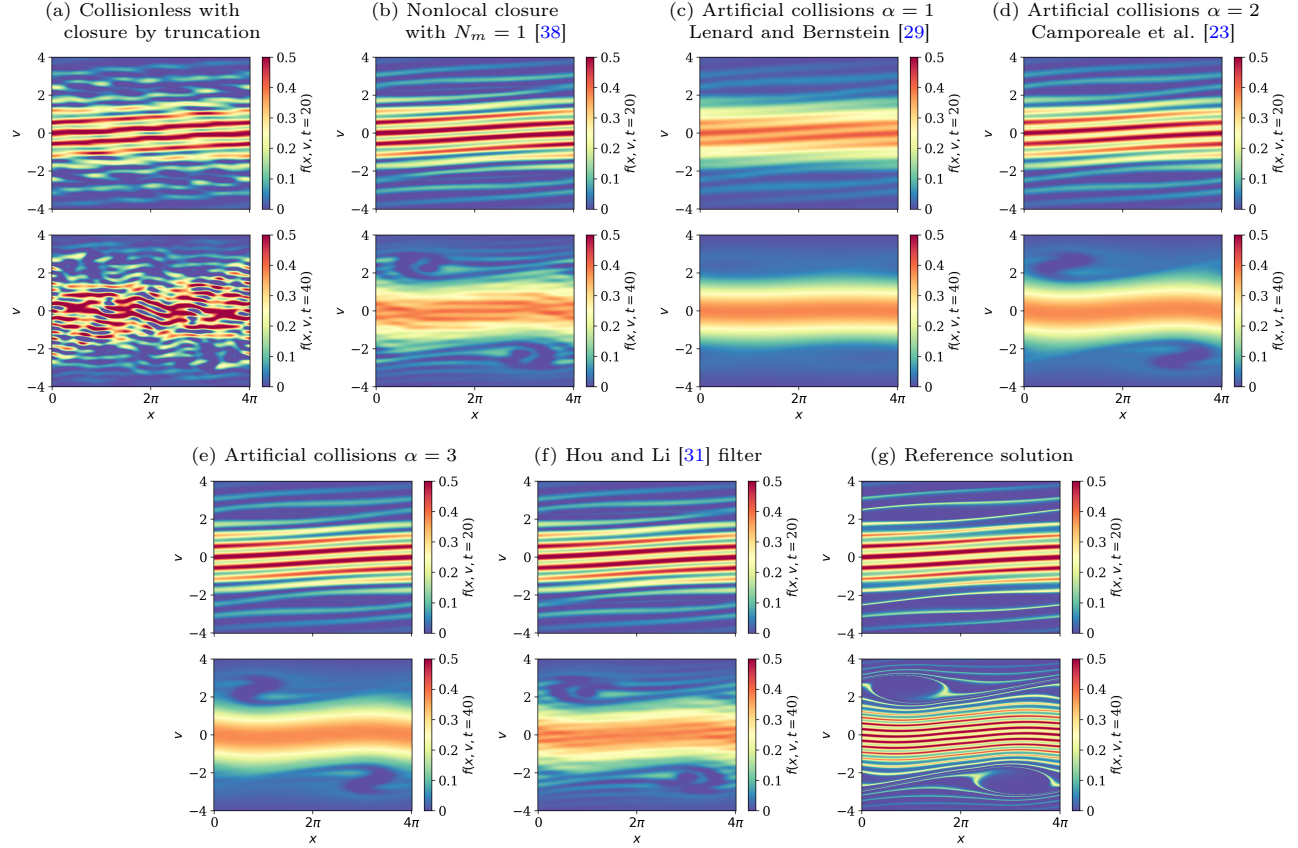


Figure 10: Nonlinear Landau damping electron distribution function $f(x, v, t)$ at time instances $t = 20$ and $t = 40$ with $N_v = 300$. Each method is compared to the reference solution in subfigure (g), which is obtained using a high-resolution finite difference scheme. While the velocity resolution of $N_v = 300$ is insufficient to fully resolve the filamentation at $t = 40$, all simulations besides the collisionless with closure by truncation in subfigure (a) and LB collisions in subfigure (c) capture the correct particle trapping vortex around the phase speed $\omega_r/k = \pm 2.8$.

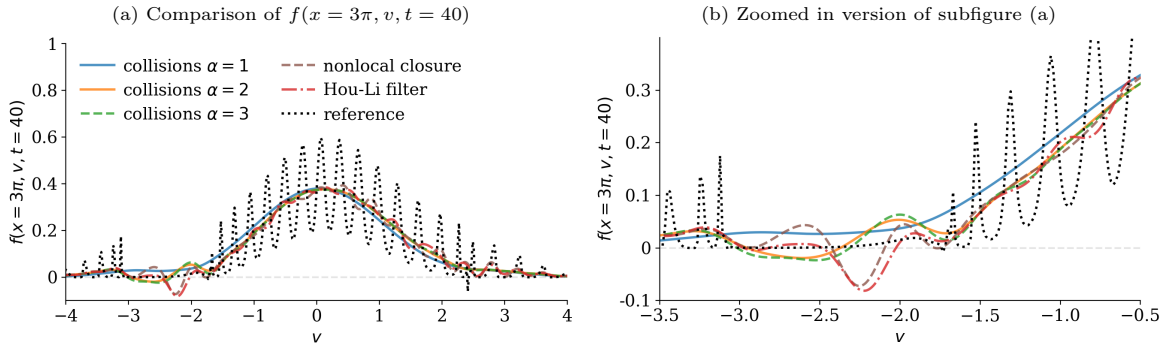


Figure 11: Cross-section of the nonlinear Landau damping electron distribution function $f(x = 3\pi, v, t = 40)$ with $N_v = 300$, shown for (a) $v \in [-4, 4]$ and (b) a zoomed-in view with $v \in [-3.5, -0.5]$. All methods, except for artificial collisions with $\alpha = 1$, produce a smoothed approximation of the reference solution. However, in the region $-3 \leq v \leq -2$, these methods result in negative values for the distribution function.

distributions, the finite AW Hermite expansion would approximate both the equilibrium and perturbation components, whereas the zeroth term in the AW Hermite expansion represents exactly a Maxwellian equilibrium. Additionally, other spectral discretizations, such as the Legendre basis, may be well-suited for non-Maxwellian distributions, which similarly to the AW Hermite basis also exhibit fluid-kinetic coupling properties [60].

Appendix A. Klimas Filter

Klimas [30] proposed to solve for an exponentially filtered distribution function

$$\bar{f}(x, v, t) := \int_{\mathbb{R}} \Theta(v - v') f(x, v', t) dv', \quad \text{where} \quad \Theta(v) := \frac{1}{\sqrt{2\pi}v_0} \exp\left(-\frac{1}{2} \left(\frac{v}{v_0}\right)^2\right).$$

The exponentially filtered Vlasov-Poisson equations (1)–(2) become

$$\begin{aligned} \left(\frac{\partial}{\partial t} + v \frac{\partial}{\partial x} + \frac{\partial \phi(x, t)}{\partial x} \frac{\partial}{\partial v}\right) \bar{f}(x, v, t) &= -v_0^2 \frac{\partial^2}{\partial x \partial v} \bar{f}(x, v, t), \\ -\frac{\partial^2 \phi(x, t)}{\partial x^2} &= 1 - \int_{\mathbb{R}} \bar{f}(x, v, t) dv. \end{aligned}$$

The filter modifies only the right-hand side of the Vlasov equation, introducing a second derivative that combines velocity and spatial derivatives. Additionally, the charge density and current density are invariant under filtering, i.e. $\int_{\mathbb{R}} f(x, v, t) dv = \int_{\mathbb{R}} \bar{f}(x, v, t) dv$ and $\int_{\mathbb{R}} v f(x, v, t) dv = \int_{\mathbb{R}} v \bar{f}(x, v, t) dv$, such that the evolution of the electric field remains unchanged for any value of $v_0 \in \mathbb{R}$ [30]. By applying the AW Hermite discretization in velocity, Fourier discretization in space, and using the recursive property in Eq. (12), we obtain

$$-v_0^2 \frac{\partial^2}{\partial x \partial v} \bar{f} \quad \Rightarrow \quad ikv_0^2 \sqrt{n} \hat{C}_{n-1}.$$

Because the Klimas filter does not correspond to a true dissipation, the Landau root is not represented by a discrete mode as in the cases considered in the main text. We have therefore tested it with dynamical simulations with different values of v_0 and found that recurrence effects are not eliminated when the Klimas filter is applied to the AW Hermite discretization with closure by truncation. Indeed, Klimas and Viñas [32] show that the Klimas filter can suppress recurrence in doubly Fourier-transformed solvers with imposed proper boundary conditions. Note that it is important to maintain $v_0 \lesssim 1$ since the convolution of two Gaussian distributions is $\mathcal{G}(\mu_1, \sigma_1) * \mathcal{G}(\mu_2, \sigma_2) = \mathcal{G}(\mu_1 + \mu_2, \sqrt{\sigma_1^2 + \sigma_2^2})$, such that setting the parameter v_0 much greater than the electron thermal velocity results in oversmoothing of the solution and the same eigenvalue analysis performed in section 3.5 predicts discrete unstable modes.

Code Availability

The public repository https://github.com/opaliss/Vlasov_Hermite_recurrence_study.git contains a collection of Jupyter notebooks and modules in Python 3.9 with the code used in this study.

Acknowledgment

O.I. appreciates the useful and informative discussions with Federico Halpern and Chris Holland. O.I. was partially supported by the Los Alamos National Laboratory (LANL) Student Fellowship sponsored by the Center for Space and Earth Science (CSES). CSES is funded by LANL’s Laboratory Directed Research and Development (LDRD) program under project number 20210528CR. The LANL LDRD Program supported O.I., G.L.D., O.K., and O.C. under project number 20220104DR. LANL is operated by Triad National Security, LLC, for the National Nuclear Security Administration of the US Department of Energy (Contract No. 89233218CNA000001).

References

- [1] F. C. Grant and M. R. Feix. Fourier-Hermite Solutions of the Vlasov Equations in the Linearized Limit. *The Physics of Fluids*, 10(4):696–702, 1967.
- [2] J. Canosa, J. Gazdag, and J. E. Fromm. The recurrence of the initial state in the numerical solution of the Vlasov equation. *Journal of Computational Physics*, 15(1):34–45, 1974.
- [3] C. Z. Cheng and G. Knorr. The integration of the Vlasov equation in configuration space. *Journal of Computational Physics*, 22(3):330–351, 1976.
- [4] J. W. Schumer and J. P. Holloway. Vlasov Simulations Using Velocity-Scaled Hermite Representations. *Journal of Computational Physics*, 144(2):626–661, 1998.
- [5] M. Shoucri and R. R. J. Gagne. Numerical solution of the Vlasov equation by transform methods. *Journal of Computational Physics*, 21(2):238–242, 1976.
- [6] H. Grad. On the kinetic theory of rarefied gases. *Communications on Pure and Applied Mathematics*, 2(4):331–407, 1949.
- [7] G. Joyce, G. Knorr, and H. K. Meier. Numerical integration methods of the Vlasov equation. *Journal of Computational Physics*, 8(1):53–63, 1971.
- [8] T. P. Armstrong. Numerical Studies of the Nonlinear Vlasov Equation. *The Physics of Fluids*, 10(6):1269–1280, 1967.
- [9] C. Black, K. Germaschewski, A. Bhattacharjee, and C. S. Ng. Discrete kinetic eigenmode spectra of electron plasma oscillations in weakly collisional plasma: A numerical study. *Physics of Plasmas*, 20(1):012125, 2013.
- [10] O. Issan, O. Koshkarov, F. D. Halpern, B. Kramer, and G. L. Delzanno. Anti-symmetric and positivity preserving formulation of a spectral method for Vlasov-Poisson equations. *Journal of Computational Physics*, 514:113263, 2024.
- [11] O. Chapurin, O. Koshkarov, G. L. Delzanno, V. Roytershteyn, P. Brady, R. Chiodi, C. Harnish, and D. Livescu. Hybrid particle-spectral method for kinetic plasma simulations. *Physics of Plasmas*, 31(2):023903, 2024.
- [12] C. Pagliantini, G. L. Delzanno, and S. Markidis. Physics-based adaptivity of a spectral method for the Vlasov-Poisson equations based on the asymmetrically-weighted Hermite expansion in velocity space. *Journal of Computational Physics*, 488:112252, 2023.
- [13] C. Pagliantini, G. Manzini, O. Koshkarov, G. L. Delzanno, and V. Roytershteyn. Energy-conserving explicit and implicit time integration methods for the multi-dimensional Hermite-DG discretization of the Vlasov-Maxwell equations. *Computer Physics Communications*, 284:108604, 2023.
- [14] E. Camporeale, G. L. Delzanno, G. Lapenta, and W. Daughton. New approach for the study of linear Vlasov stability of inhomogeneous systems. *Physics of Plasmas*, 13(9):092110, 2006.
- [15] G. L. Delzanno. Multi-dimensional, fully-implicit, spectral method for the Vlasov-Maxwell equations with exact conservation laws in discrete form. *Journal of Computational Physics*, 301:338–356, 2015.
- [16] O. Koshkarov, G. Manzini, G. L. Delzanno, C. Pagliantini, and V. Roytershteyn. The multi-dimensional Hermite-discontinuous Galerkin method for the Vlasov-Maxwell equations. *Computer Physics Communications*, 264:107866, 2021.
- [17] V. Roytershteyn and G. L. Delzanno. Spectral Approach to Plasma Kinetic Simulations Based on Hermite Decomposition in the Velocity Space. *Frontiers in Astronomy and Space Sciences*, 5, 2018.
- [18] G. Celebre, S. Servidio, and F. Valentini. Phase space dynamics of unmagnetized plasmas: Collisionless and collisional regimes. *Physics of Plasmas*, 30(9):092304, 2023.

- [19] O. Pezzi, F. Valentini, S. Servidio, E. Camporeale, and P. Veltri. Fourier-Hermite decomposition of the collisional Vlasov-Maxwell system: implications for the velocity-space cascade. *Plasma Physics and Controlled Fusion*, 61(5):054005, 2019.
- [20] O. Pezzi, E. Camporeale, and F. Valentini. Collisional effects on the numerical recurrence in Vlasov-Poisson simulations. *Physics of Plasmas*, 23(2), 2016.
- [21] S. Le Bourdieu, F. de Vuyst, and L. Jacquet. Numerical solution of the Vlasov-Poisson system using generalized Hermite functions. *Computer Physics Communications*, 175(8):528–544, 2006.
- [22] N. F. Loureiro, W. Dorland, L. Foz de Feliciano, A. Kanekar, A. Mallet, M. S. Vilelas, and A. Zocco. Viriato: A Fourier-Hermite spectral code for strongly magnetized fluid-kinetic plasma dynamics. *Computer Physics Communications*, 206:45–63, 2016.
- [23] E. Camporeale, G. L. Delzanno, B. K. Bergen, and J. D. Moulton. On the velocity space discretization for the Vlasov-Poisson system: Comparison between implicit Hermite spectral and Particle-in-Cell methods. *Computer Physics Communications*, 198:47–58, 2016.
- [24] G. W. Hammett, M. A. Beer, W. Dorland, S. C. Cowley, and S. A. Smith. Developments in the gyrofluid approach to tokamak turbulence simulations. *Plasma Physics and Controlled Fusion*, 35(8):973, 1993.
- [25] J. P. Boyd. *Chebyshev and Fourier spectral methods*. Courier Corporation, 2001.
- [26] L. D. Landau. On the vibrations of the electronic plasma. *Journal of Physics*, 10(1):25–34, 1946.
- [27] C. S. Ng, A. Bhattacharjee, and F. Skiff. Kinetic Eigenmodes and Discrete Spectrum of Plasma Oscillations in a Weakly Collisional Plasma. *Phys. Rev. Lett.*, 83:1974–1977, 1999.
- [28] C. S. Ng, A. Bhattacharjee, and F. Skiff. Complete spectrum of kinetic eigenmodes for plasma oscillations in a weakly collisional plasma. *Phys. Rev. Lett.*, 92:065002, 2004.
- [29] A. Lenard and I. B. Bernstein. Plasma Oscillations with Diffusion in Velocity Space. *Phys. Rev.*, 112:1456–1459, 1958.
- [30] A. J. Klimas. A method for overcoming the velocity space filamentation problem in collisionless plasma model solutions. *Journal of Computational Physics*, 68(1):202–226, 1987.
- [31] T. Y. Hou and R. Li. Computing nearly singular solutions using pseudo-spectral methods. *Journal of Computational Physics*, 226(1):379–397, 2007.
- [32] A. J. Klimas and A. F. Viñas. Absence of recurrence in Fourier-Fourier transformed Vlasov-Poisson simulations. *Journal of Plasma Physics*, 84(4):905840405, 2018.
- [33] Z. Cai and Y. Wang. Suppression of recurrence in the Hermite-spectral method for transport equations. *SIAM Journal on Numerical Analysis*, 56(5):3144–3168, 2018.
- [34] Y. Di, Y. Fan, Z. Kou, R. Li, and Y. Wang. Filtered hyperbolic moment method for the Vlasov equation. *Journal of Scientific Computing*, 79:969–991, 2019.
- [35] F. Filbet and T. Xiong. Conservative discontinuous Galerkin/Hermite spectral method for the Vlasov-Poisson system. *Communications on Applied Mathematics and Computation*, pages 1–26, 2022.
- [36] G. W. Hammett and F. W. Perkins. Fluid moment models for Landau damping with application to the ion-temperature-gradient instability. *Phys. Rev. Lett.*, 64:3019–3022, 1990.
- [37] G. W. Hammett, W. Dorland, and F. W. Perkins. Fluid models of phase mixing, Landau damping, and nonlinear gyrokinetic dynamics. *Physics of Fluids B: Plasma Physics*, 4(7):2052–2061, 1992.
- [38] S. A. Smith. Dissipative closures for statistical moments, fluid moments, and subgrid scales in plasma turbulence. *PhD Thesis*, 1997.
- [39] S. P. Gary. *Theory of Space Plasma Microinstabilities*. Cambridge University Press, 1993.

- [40] P. Hunana, A. Tenerani, G. P. Zank, M. L. Goldstein, G. M. Webb, E. Khomenko, M. Collados, P. S. Cally, L. Adhikari, and M. Velli. An introductory guide to fluid models with anisotropic temperatures. Part 2. Kinetic theory, Padé approximants and Landau fluid closures. *Journal of Plasma Physics*, 85(6):205850603, 2019.
- [41] R. Fitzpatrick. *Plasma Physics: An Introduction*. CRC Press, 2015.
- [42] B. D. Fried and S. D. Conte. *The Plasma Dispersion Function; the Hilbert Transform of the Gaussian*. Academic Press, 1961.
- [43] J. T. Parker and P. J. Dellar. Fourier-Hermite spectral representation for the Vlasov-Poisson system in the weakly collisional limit. *Journal of Plasma Physics*, 81(2):305810203, 2015.
- [44] M. Abramowitz and I. A. Stegun. *Handbook of Mathematical Functions: With Formulas, Graphs, and Mathematical Tables*. Applied mathematics series. Dover Publications, 1965.
- [45] C. Gillot, G. Dif-Pradalier, X. Garbet, P. Ghendrih, V. Grandgirard, and Y. Sarazin. Model order reduction approach to the one-dimensional collisionless closure problem. *Physics of Plasmas*, 28(2):022111, 2021.
- [46] J. Vencels, G. L. Delzanno, A. Johnson, I. Peng, E. Laure, and S. Markidis. Spectral Solver for Multi-Scale Plasma Physics Simulations with Dynamically Adaptive Number of Moments. *Procedia Computer Science*, 51:1148–1157, 2015.
- [47] J. T. Parker. Gyrokinetic simulations of fusion plasmas using a spectral velocity space representation. *PhD Thesis*, 2016.
- [48] H. Gajewski and K. Zacharias. On the convergence of the Fourier-Hermite transformation method for the Vlasov equation with an artificial collision term. *Journal of Mathematical Analysis and Applications*, 61(3):752–773, 1977.
- [49] M. J. Pueschel, T. Dannert, and F. Jenko. On the role of numerical dissipation in gyrokinetic Vlasov simulations of plasma microturbulence. *Computer Physics Communications*, 181(8):1428–1437, 2010.
- [50] T. Passot and A. Pouquet. Hyperviscosity for compressible flows using spectral methods. *Journal of Computational Physics*, 75(2):300–313, 1988.
- [51] D. Funaro and G. Manzini. Stability and conservation properties of Hermite-based approximations of the Vlasov-Poisson system. *Journal of Scientific Computing*, 88(1):29, 2021.
- [52] M. Bessemoulin-Chatard and F. Filbet. On the stability of conservative discontinuous Galerkin/Hermite spectral methods for the Vlasov-Poisson system. *Journal of Computational Physics*, 451:110881, 2022.
- [53] B. Eliasson. Outflow boundary conditions for the Fourier transformed one-dimensional Vlasov-Poisson system. *Journal of scientific computing*, 16(1):1–28, 2001.
- [54] A. M. Dimits, I. Joseph, and M. V. Umansky. A fast non-Fourier method for Landau-fluid operators. *Physics of Plasmas*, 21(5):055907, 2014.
- [55] D. A. Knoll and D. E. Keyes. Jacobian-free Newton-Krylov methods: a survey of approaches and applications. *Journal of Computational Physics*, 193(2):357–397, 2004.
- [56] T. Shiroto, N. Ohnishi, and Y. Sentoku. Quadratic conservative scheme for relativistic Vlasov-Maxwell system. *Journal of Computational Physics*, 379:32–50, 2019.
- [57] T. Jikei and T. Amano. A non-local fluid closure for modeling cyclotron resonance in collisionless magnetized plasmas. *Physics of Plasmas*, 28(4):042105, 2021.
- [58] K. Fan, X. Xu, B. Zhu, and P. Li. Kinetic Landau-fluid closures of non-Maxwellian distributions. *Physics of Plasmas*, 29(4):042116, 2022.
- [59] V. Pierrard and M. Lazar. Kappa distributions: Theory and applications in space plasmas. *Solar physics*, 267:153–174, 2010.
- [60] G. Manzini, G. L. Delzanno, J. Vencels, and S. Markidis. A Legendre-Fourier spectral method with exact conservation laws for the Vlasov-Poisson system. *Journal of Computational Physics*, 317:82–107, 2016.